Multi-scale and multi-technique analysis of the thermal degradation of poly(ether ether ketone)

Emilie Courvoisier, Yoann Bicaba, Xavier Colin

Multi-scale and multi-technique analysis of the thermal degradation of poly (ether ether ketone)

Emilie Courvoisier[a,b], Yoann Bicaba[a], Xavier Colin[b,*]

[a] SAFRAN Composites, 33 avenue de la gare, 97601, Itteville, France
[b] Laboratoire PIMM, Arts et Metiers ParisTech, 151 boulevard de l'Hôpital, 75013, Paris, France

ARTICLE INFO

Keywords:
PEEK
Thermal oxidation
Chain scissions
Crosslinking
Young's modulus

ABSTRACT

The thermal degradation of PEEK has been studied in rubbery state in wide ranges of temperature (between 180 and 320 °C) and oxygen partial pressure (between 0.21 and 50 bars). On one hand, the thermal ageing mechanisms have been analysed and elucidated by FTIR spectrophotometry and by differential scanning calorimetry (DSC) on sufficiently thin PEEK films (between 10 and 60 μm thickness) to be totally free of the effects of oxygen diffusion. Oxidation occurs on aromatic rings causing the growth of five new IR absorption bands centered at 3650, 3525, 1780, 1740 et 1718 cm^{-1} and attributed to the stretching vibrations of the O-H bonds of phenol and benzoïc acid, and the C-O bonds of benzoïc anhydride, phenyl benzoate and fluorenone respectively. In addition, oxidation leads to a large predominance of crosslinking over chain scissions resulting in a sharp increase of T_g. This reduction in molecular mobility prevents the annealing of PEEK, in particular when the temperature of exposure is higher than the onset of the melting endotherm. On the other hand, the consequences of oxidation on the elastic properties have been analysed and elucidated by micro-indentation on polished cross-sections of PEEK plates of 3 mm thickness. The diffusion control of oxidation leads to the development of profiles of Young's modulus within the sample thickness, which correlate perfectly with the changes in crystallinity and macromolecular architecture determined at lower scales. The validity of the Tobolsky's relationship is demonstrated.

1. Introduction

The competition in the aeronautical market depends both on economic and ecological issues such as the reduction of costs, on-board weight and fuel consumption. That is the reason why since its origin, the aerospace industry has been looking for new lighter materials with high thermo-mechanical properties. In this context, the use of composite materials made of organic matrix reinforced with glass or carbon fibers (OMC) has been amplified with the aim of progressively replacing the metallic materials. Initially designed for the fabrication of structural parts (wing, tail, fuselage, etc.), OMCs are now being considered for applications in increasingly harsh thermo-chemical environments, such as areas near heat sources (typically in environments of aircraft engine). However, they will be used only if their long-term durability is clearly demonstrated.

The use of thermoplastic matrices has several advantages, such as the integration of specific functions, but also the assembly of parts of the same or different nature. Among the thermoplastic matrices that can meet the aeronautical specifications, poly(ether ether ketone) (PEEK) appears as a serious candidate. Indeed, it is a semi-crystalline polymer with a highly aromatic structure giving it not only high thermomechanical performances (glass transition temperature and melting point are $T_g \approx 153$ °C and $T_m \approx 343$ °C respectively), but also a high chemical resistance to the most usual solvents (acetone, toluene, ethyl acetate, etc.) and aeronautical fluids (in particular, Skydrol). The thermal degradation of PEEK has been studied under inert or slightly oxygenated atmosphere (typically in air), mostly in molten state (between 340 and 485 °C), but rarely in rubber state (between 300 and 320 °C) and never, to our knowledge, in glassy state.

The oxidation of PEEK occurs on the only hydrocarbon groups available in the monomer unit, i.e. on the aromatic rings, in spite of the very low lability of their H atoms. Indeed, the dissociation energy of the aromatic C-H bond is of the order of 465 kJ mol^{-1}, against 393 and 378 kJ mol^{-1} for the methylenic and methynic C-H bonds respectively [1]. Above 400 °C, oxidation would be mainly initiated by the breakdown of the ether and ketone bonds of the monomer unit [2–4]. It leads to the disappearance of the ketone groups (at 1653 cm^{-1}), but also to the formation of a wide variety of degradation products detected by FTIR spectrophotometry. They include macromolecular products such as phenols (between 3400 and 3700 cm^{-1}), phenyl benzoate (at

* Corresponding author.
E-mail address: xavier.colin@ensam.eu (X. Colin).

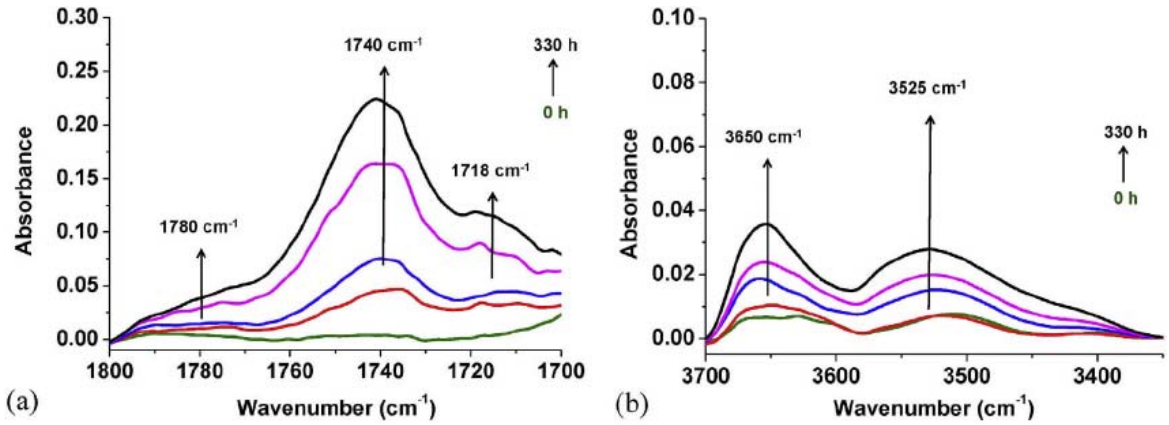

Fig. 1. Changes in the regions of C═O (a) and O-H bonds (b) in the FTIR spectrum of PEEK during its thermal ageing in air at 300 °C.

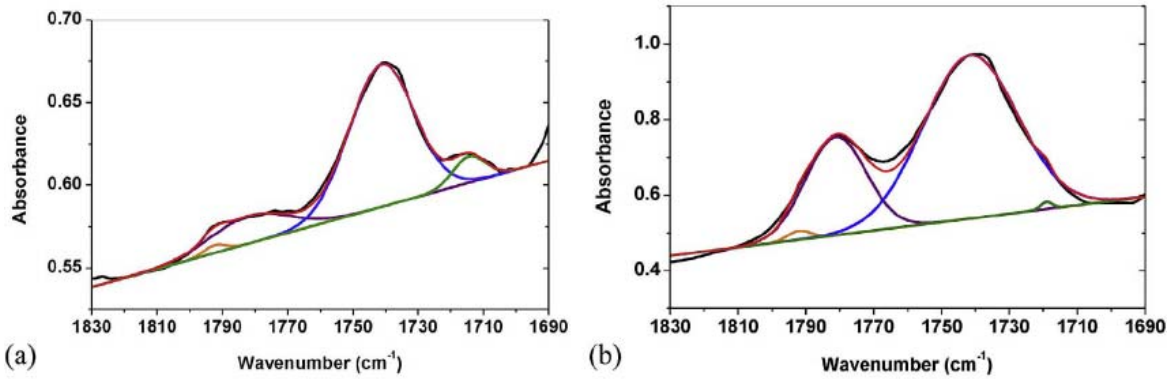

Fig. 2. Deconvolution of the region of C═O bonds in the IR spectrum of PEEK after 324 h of exposure at 300 °C under 0.21 bar of oxygen (a) and after 196 h of exposure at 250 °C under 10 bars of oxygen (b).

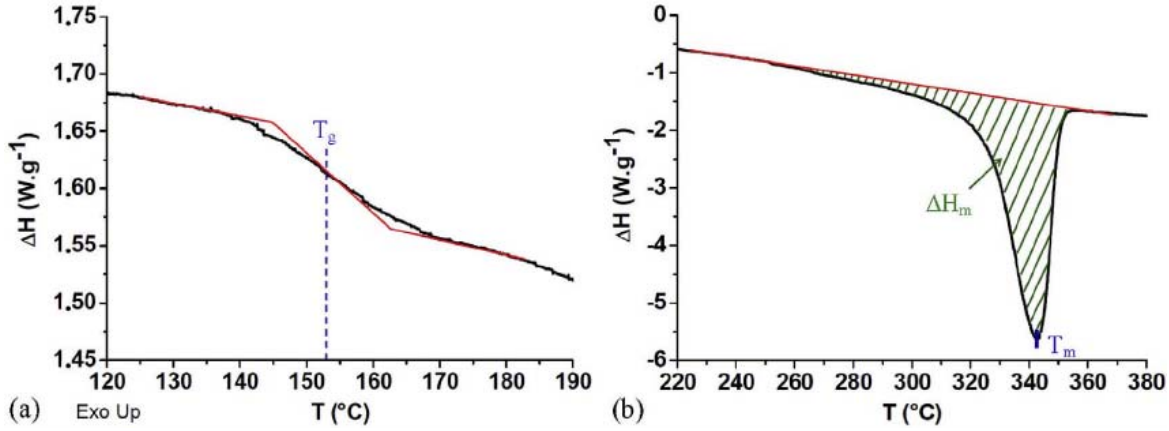

Fig. 3. DSC thermogram of unaged PEEK zoomed around the glass transition temperature (a) and the melting endotherm (b). Determination of T_g, T_m and ΔH_m.

1739 cm^{-1}) and fluorenone (1711 cm^{-1}) [2–4], but also many volatile compounds [4–6]. Hardly detectable below 430 °C, volatile compounds have been clearly evidenced above 450 °C by thermogravimetry coupled with gas chromatography (TGA-GC) or mass spectrometry (TGA-MS). They include quinones, phenols, carbon monoxide and dioxide, benzene, but also aromatic ethers and ketones [4,6].

Mechanisms which involve the rearrangement of phenoxyl and acyl radicals, resulting from the breakdown of the ether and ketone bonds respectively, have been proposed to explain the formation of most degradation products. However, these purely thermolytic mechanisms do not explain the acceleration of the oxidation kinetics when raising oxygen partial pressure. Between 360 and 460 °C, a second important source of radicals, which may also explain the accumulation of several degradation products, is the unimolecular decomposition of hydroperoxides [7].

Changes in the macromolecular architecture of PEEK have been also detected by steric exclusion chromatography (SEC or GPC) [5], and by viscometry in solution [3] or in molten state [5,7,8]. Between 300 and 485 °C, crosslinking predominates largely over chain scissions, this relative predominance being amplified when raising the oxygen partial pressure. Crosslinking causes the increase in the molecular weight [3,5,7,8], gel fraction [3,4] and glass transition temperature [5,8,9]. The most probable crosslinking mechanism is the bimolecular recombination of phenyl radicals [3–6].

Finally, the changes in the crystalline morphology of PEEK have been evidenced by differential calorimetry (DSC). Between 380 and 440 °C, crosslinking limits crystallization when PEEK is cooled to room temperature from its molten state, resulting in a decrease in both the

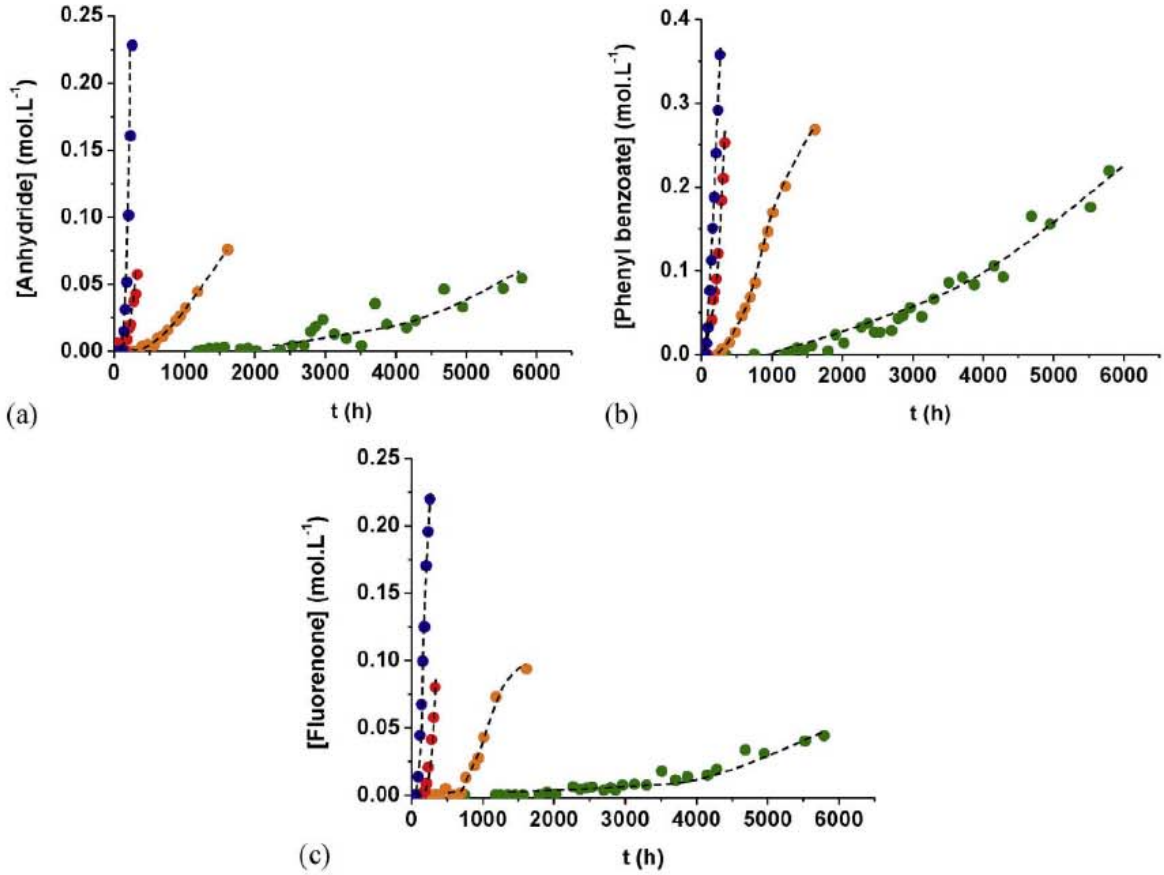

Fig. 4. Changes in the concentrations of benzoic anhydride (a), phenyl benzoate (b) and fluorenone (c) during the thermal ageing of PEEK in air at 250 (in green), 280 (orange), 300 (red) and 320 °C (blue).

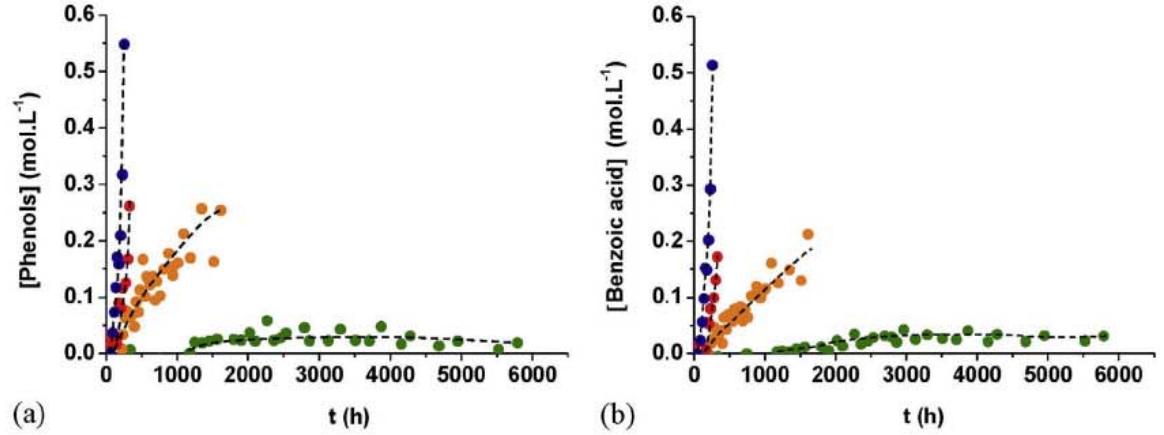

Fig. 5. Changes in the concentrations of phenols (a) and benzoic acid (b) during the thermal ageing of PEEK in air at 250 (in green), 280 (orange), 300 (red) and 320 °C (blue). (For interpretation of the references to colour in this figure legend, the reader is referred to the Web version of this article.)

Table 1
Activation energy of the induction times (t_i) and the maximum rates (r_{ox}) of the formation of benzoic anhydride, phenyl benzoate, fluorenone, phenols and benzoic acid in air between 250 and 320 °C.

Products	E_a of t_i (kJ.mol^{-1}) in air	E_a of r_{ox} (kJ.mol^{-1}) in air
Benzoic anhydride	102	177
Phenyl benzoate	106	143
Fluorenone	134	166
Phenols	102	166
Benzoic acid	92	175

melting point and crystallinity ratio [5,8,9].

The present article provides a detailed multi-scale and multi-technical analysis of the thermal degradation of PEEK at lower temperatures and higher oxygen partial pressures than those studied until now in the literature. A peculiar attention is paid to the consequences of degradation on two key thermomechanical properties in the aeronautical field: the changes in the glass transition temperature and Young's modulus.

2. Experimental

The material under study is the PEEK 150G supplied by Victrex company in the form of pellets. Plates of 3 mm thickness were molded

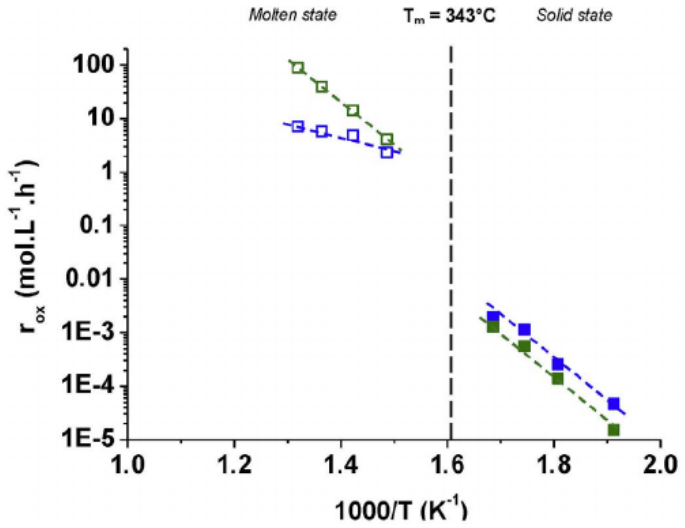

Fig. 6. Arrhenius diagram of the maximum rates (r_{ox}) of the formation of phenyl benzoate (in blue) and fluorenone (green) in air between 250 and 485 °C. The results of the present study (between 250 and 320 °C) are given in full symbols whereas those of the literature (between 400 and 485 °C [2]) are given in empty symbols. (For interpretation of the references to colour in this figure legend, the reader is referred to the Web version of this article.)

Table 2
Activation energy of the maximum rates (r_{ox}) of the formation of phenyl benzoate and fluorenone in air in rubbery state between 250 and 320 °C (present study) and in molten state between 400 and 485 °C (literature [2]).

Products	E_a of r_{ox} (kJ.mol^{-1}) in air	
	Rubbery state	Molten state
Phenyl benzoate	143	52
Fluorenone	166	153

by an injection machine from these pellets by the Pôle Européen de Plasturgie (PEP) located in Oyonnax (France). The plates were then cut with a LEICA RM2255 microtome in order to obtain sufficiently thin films (typically between 10 and 60 µm thickness) for ensuring a homogeneous oxidation throughout their thickness. The oxidation kinetics of PEEK was studied in rubber state at 180, 200, 220, 250, 280, 300 and 320 °C under oxygen partial pressures ranged between 0.21 bar (in air-ventilated ovens regulated at ± 1 °C) and 50 bars (in autoclaves). Given the high impact of oxygen partial pressure on the oxidation kinetics, the ageing experiments at the highest temperatures (typically between 280 and 320 °C) was carried out under 0.21 bar of oxygen, while those at the lowest temperatures (between 180 and 250 °C) had to be made above 1 bar of oxygen, in order to detect sufficiently significant structural changes over durations compatible with the duration of a PhD thesis work (of a few years). All the films were periodically removed from the ageing chambers and cooled to room temperature in a desiccator containing silica gel for preventing any moisture recovery prior to being characterized. It is noteworthy that much thicker samples (plates of 3 mm thickness) were also exposed in air-ventilated ovens at 280 and 300 °C in order to put in evidence the development of oxidation profiles. In all cases, the consequences of oxidation were analyzed by several complementary laboratory techniques from the molecular to the macroscopic scales, via the macromolecular, morphological and microscopic scales.

The changes in molecular structure were followed by FTIR spectrophotometry in a transmission mode. The FTIR spectra of the PEEK films were measured before and after ageing for detecting and quantifying the disappearance of chemical groups initially present in the PEEK matrix and the formation of the main oxidation products. The analyzes were carried out with a Perkin Elmer Frontier apparatus between 400 and 4000 cm^{-1}, after having averaged the 16 recordings obtained with a minimum resolution of 4 cm^{-1}. The thermal ageing of PEEK leads to two major changes in the FTIR spectrum (Fig. 1). On the one hand, in the hydroxyl zone between 3400 and 3700 cm^{-1}, it can be seen the appearance and growth of two IR absorption bands centered at 3600 and 3525 cm^{-1}. They are respectively attributed to the elongation vibrations of the O-H bonds of phenols and all other types of hydroxyl products, mostly benzoic acid [2,10]. On the other hand, in the carbonyl zone between 1700 and 1800 cm^{-1}, it is observed the appearance and growth of three IR absorption bands centered at 1780, 1740 and 1718 cm^{-1}. They are respectively attributed to the elongation vibrations of the C-O bonds of benzoic anhydride, phenyl benzoate and fluorenone [2,10,11].

Let us recall that the concentration C of these various products is related to the absorbance Abs of their IR absorption band according to the Beer-Lambert's law:

$$C = \frac{Abs}{e \times \varepsilon} \quad (1)$$

where e is the sample thickness (expressed in cm) and ε the coefficient of molar extinction whose averaged values are given in the literature: ε(O-H of phenols and acids) = 90 L mol^{-1}.cm^{-1} [12] [13], ε (C═O of anhydrides and ketones) = 300 L mol^{-1}.cm^{-1} [14] and ε (C═O of esters) = 550 L mol^{-1}.cm^{-1} [15].

It should be pointed that, due to the overlap of the IR absorption bands in the carbonyl region, it was necessary to carry out a mathematical deconvolution based on Gaussian functions with the OriginLab software for extracting the elementary contributions of the various carbonyl groups (Fig. 2). In addition to the three previous bands, this deconvolution has put in evidence a fourth contribution around 1790 cm^{-1}. However, since its absorbance is extremely low and does not evolve during the thermal ageing, this latter band was logically neglected thereafter.

The consequences of oxidation on the macromolecular architecture and crystalline morphology of PEEK were followed by differential calorimetry (DSC). The DSC thermograms of the PEEK films were

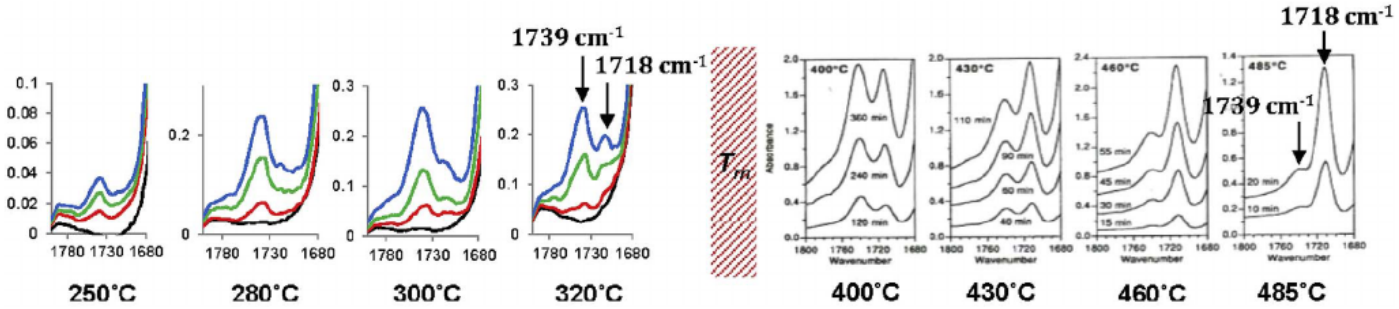

Fig. 7. Relative predominance of the IR absorption bands of phenyl benzoate (at 1740 cm^{-1}) and fluorenone (1718 cm^{-1}) during the thermal ageing of PEEK in air in rubbery state between 250 and 320 °C (present study) and in molten state between 400 and 485 °C (literature [2]).

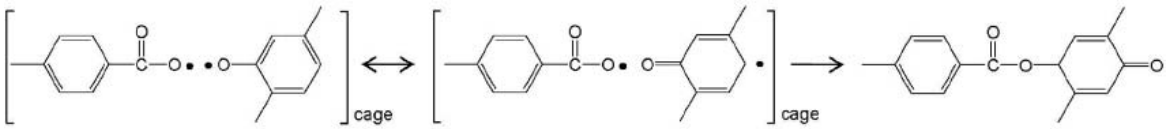

Fig. 8. Formation mechanism of phenyl benzoate by coupling carboxyl and phenoxyl radicals.

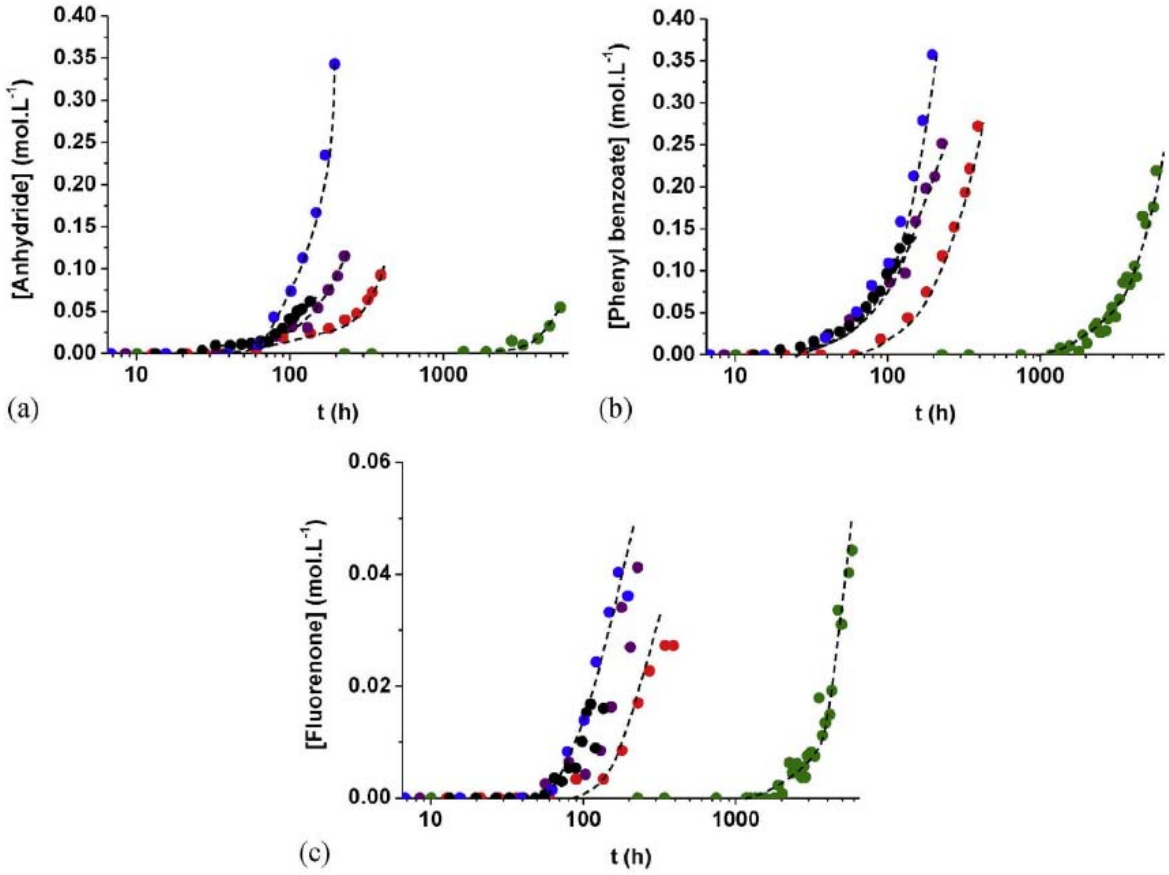

Fig. 9. Changes in the concentrations of benzoic anhydride (a), phenyl benzoate (b) and fluorenone (c) during the thermal ageing of PEEK under an oxygen pressure of 0.21 bar (in green), 3 bars (red), 6 bars (violet), 8 bars (black) and 10 bars (blue) at 250 °C. (For interpretation of the references to colour in this figure legend, the reader is referred to the Web version of this article.)

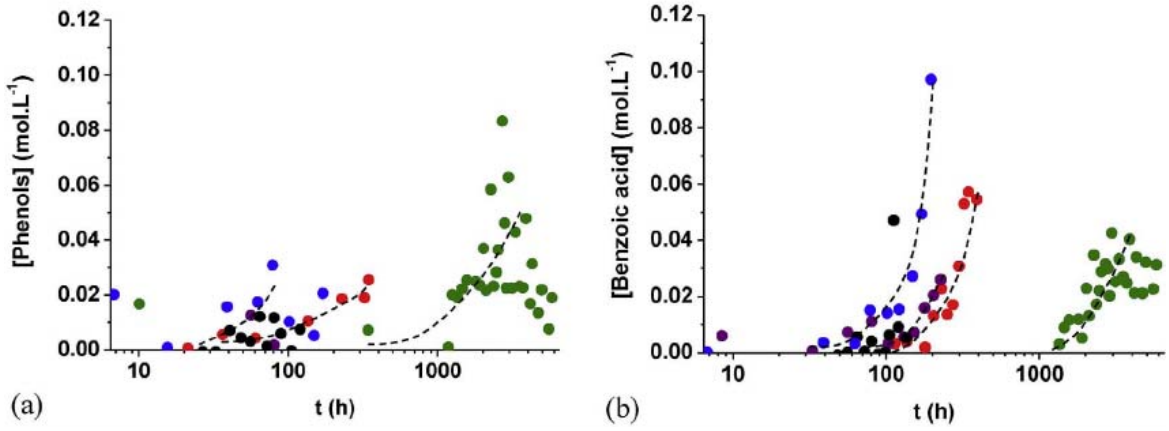

Fig. 10. Changes in the concentrations of phenols (a) and benzoic acid (b) during the thermal ageing of PEEK under an oxygen pressure of 0.21 bar (in green), 3 bars (red), 6 bars (violet), 8 bars (black) and 10 bars (blue) at 250 °C. (For interpretation of the references to colour in this figure legend, the reader is referred to the Web version of this article.)

measured before and after thermal ageing for accessing the changes in the glass transition temperature (T_g), melting point (T_m) and melting enthalpy (ΔH_m). The analyzes were carried out with a TA Instruments Q1000 calorimeter between 25 and 300 °C with a heating rate of 10 °C.min^{-1} under a nitrogen flow. As shown in Fig. 3, the values of T_g and T_m were respectively taken at the inflection point and at the top of the endothermic peak of the variation curve of the heat flux with the temperature. The value of ΔH_m corresponds to the area under the endothermic peak.

The crystallinity ratio was determined with the following classical

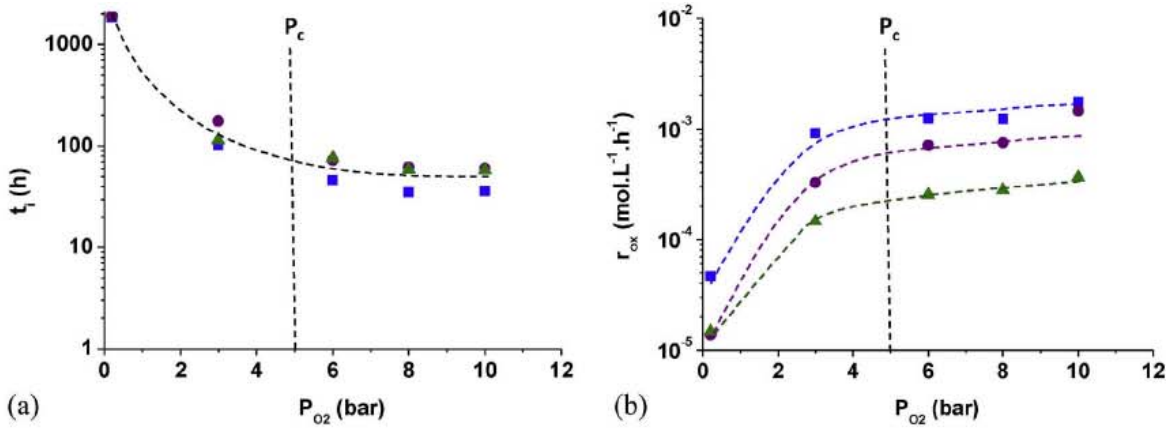

Fig. 11. Changes of the induction times (a) and the maximum rates (b) of the formation of benzoic anhydride (●), phenyl benzoate (■) and fluorenone (▲) with the oxygen partial pressure at 250 °C.

Table 3
Critical pressure (P_C), induction time (t_i) and maximum rate (r_{ox}) of the formation of benzoic anhydride, phenyl benzoate and fluorenone in oxygen excess at 220 and 250 °C.

Products	T (°C)	P_c (bars)	t_i in O_2 excess (h)	r_{ox} in O_2 excess (mol.L^{-1}.h^{-1})
Benzoic anhydride	220	20	227	8.2 10^{-4}
Phenyl benzoate			262	8.4 10^{-4}
Fluorenone			250	0.97 10^{-4}
Benzoic anhydride	250	5	62	19.7 10^{-4}
Phenyl benzoate			39	13.1 10^{-4}
Fluorenone			64	4.3 10^{-4}

equation:

$$X_C\,(\%) = \frac{\Delta H_m}{\Delta H_{m0}} \times 100 \qquad (2)$$

where ΔH_{m0} is the melting enthalpy of the crystal: $\Delta H_{m0} = 130\ J\ g^{-1}$ for PEEK [16].

The thickness of the crystalline lamellae was determined with the Gibbs-Thomson's relationship:

$$l_C = \frac{2\sigma_e T_{f0}}{\rho_C \Delta H_{m0}(T_{m0} - T_m)} \qquad (3)$$

where σ_e is the free surface energy at the interface between the amorphous and crystalline phases, ρ_C is the density of the crystalline phase and T_{m0} is the melting point of the perfect crystal: $\sigma_e = 4.9 \times 10^{-2}\ J\ m^{-2}$, $\rho_C = 1400\ kg\ m^{-3}$ and $T_{m0} = 668\ K$ for PEEK [16]. However, since there is no clear correlation between the changes in l_C and the changes measured at all the other structural scales, in first approach, only the X_C results will be reported in the present article.

Finally, the impact of thermal ageing on the elastic properties (in particular, on the Young's modulus) of PEEK was determined by micro-indentation on the polished cross-sections of PEEK plates of 3 mm thickness. The plates were cut in the thickness direction and embedded in a commercial acrylic KM-V resin, which was crosslinked for 12 h under primary vacuum at room temperature. Then, the plate cross-sections were polished with a MECAPOL P320 device using silicon carbide abrasive papers of decreasing particle size (typically from 80 to

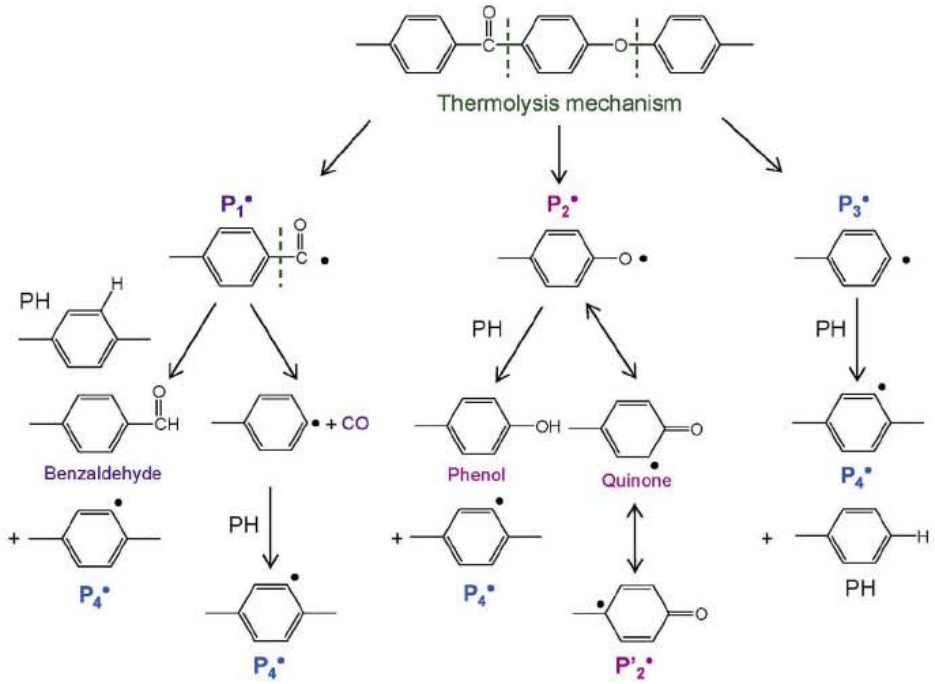

Fig. 12. Initiation of the thermal degradation of PEEK by thermolytic breakdown of ketone and ether bonds of the macromolecular chain. Formation of several radical species denoted: $P_1^{\bullet}$, $P_2^{\bullet}$, $P_3^{\bullet}$ and $P_4^{\bullet}$.

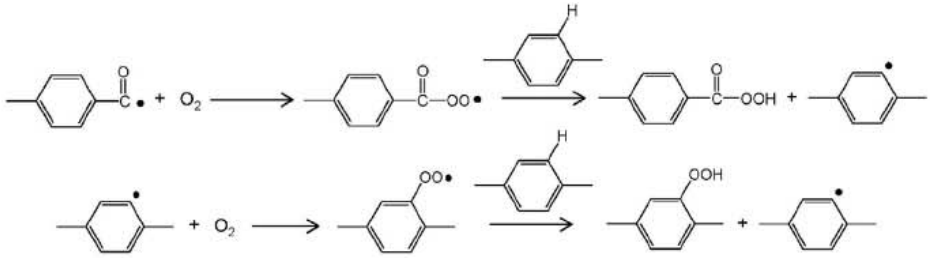

Fig. 13. Oxygen addition onto acyl and phenyl radicals followed by the formation of hydroperoxides by hydrogen abstraction on aromatic rings.

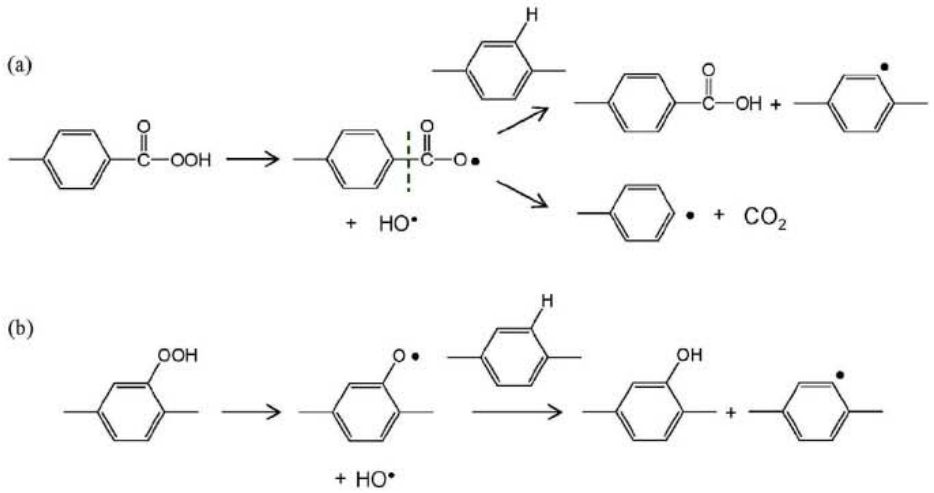

Fig. 14. Initiation of the thermal degradation by unimolecular decomposition of hydroperoxide: a) Resulting from acyl radical and leading to the formation of benzoic acid (top) or decarboxylation (below); b) Resulting from phenyl radical and leading to the formation of phenol.

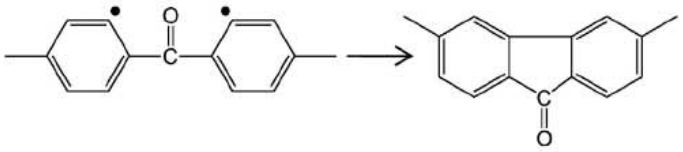

Fig. 15. Formation mechanism of fluorenone by intramolecular coupling of phenyl radicals.

2400 granulometry). Finally, a mirror finish was obtained using diamond pastes of decreasing particle size (typically from 3 to 0.25 µm). The indentations were then performed with a CSM Instrument Micro Indenter equipped with a Vickers diamond tip of pyramidal geometry, with a force of 500 mN and a loading and unloading rate of 1000 µm min^{-1}. A pause of 5 s was systematically applied between the loading and unloading. The Indentation 4.37 operating software gives directly the value of the reduced modulus E_r of the material, which is calculated according to Oliver & Pharr's method [17–19]:

$$E_r = \frac{\sqrt{\pi}\,S}{2\beta\sqrt{A_c}} \tag{4}$$

where S is the initial slope of the unloading curve, β is a shape factor depending on the indenter type (β = 1.012 for a Vickers tip) and A_c is the contact area, between the indenter and the sample, projected perpendicularly to the indenter axis on the sample surface: $A_C = a^2$, a being the side length of the projected square. This latter quantity is also directly given by the operating software. It depends both on the penetration depth of the indenter and the indenter geometry.

Then, the local elastic modulus E was determined from the reduced modulus E_r with the following equation:

$$E = \frac{1}{\frac{1-\nu^2}{E_r} - \frac{1-\nu_i 2}{E_i}} \tag{5}$$

where ν is the Poisson's coefficient of the virgin PEEK: $\nu = 0.4$ (supplier data), and ν_i and E_i are respectively the Poisson's coefficient and Young's modulus of the diamond indenter: $\nu_i = 0.07$ and $E_i = 1141$ GPa.

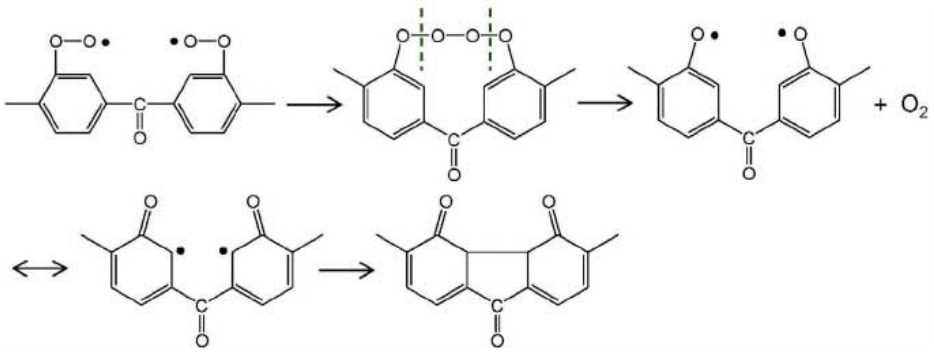

Fig. 16. Formation mechanism of fluorenone by intramolecular coupling of peroxy radicals.

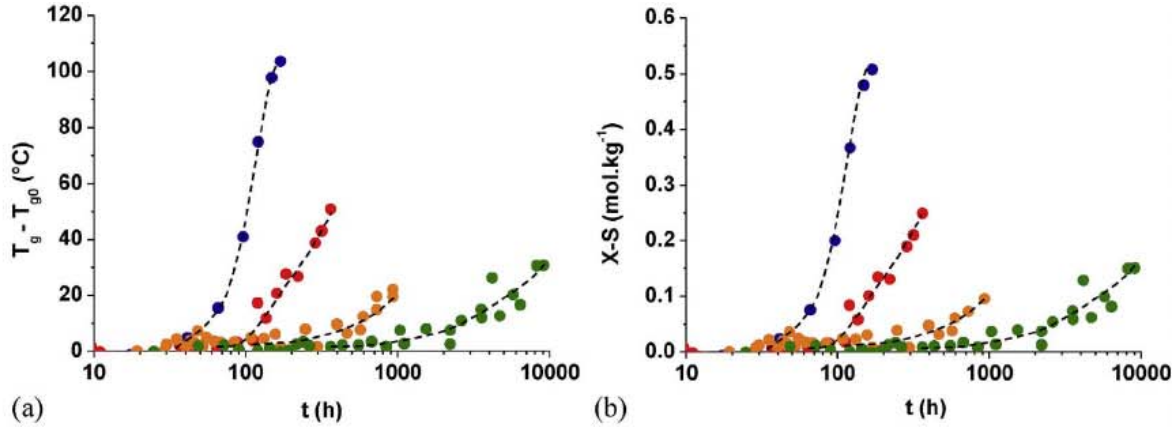

Fig. 17. Differences between the glass transition temperature and its initial value (T_g - T_{g0}) (a) and between the numbers of crosslinking and chain scission events (X - S) (b) during the thermal ageing of PEEK in air at 250 (in green), 280 (orange), 300 (red) and 320 °C (blue). (For interpretation of the references to colour in this figure legend, the reader is referred to the Web version of this article.)

Table 4
Activation energy of induction times (t_i) and maximum rates (r) for molar and macromolecular modifications in air between 250 and 320 °C.

	E_a of t_i (kJ.mol^{-1}) in air	E_a of r (kJ.mol^{-1}) in air
Benzoic anhydride	102	177
Phenyl benzoate	106	143
Fluorenone	134	166
Crosslinking	113	220

The global elastic modulus E_S of the sample is the average value of the N local values E(j) constituting the micro-indentation profile:

$$E_S = \frac{1}{N}\sum_{j=1}^{N} E(j) \tag{6}$$

In this study, E_S was used as the Young's modulus of the sample after having checked, by uniaxial tensile testing, that it gives a very good estimate of this latter. Indeed, it has been found that their respective values differ only by a factor of 0.84.

3. Results and discussion

3.1. Changes in molecular structure

As an example, Fig. 4 and Fig. 5 report the changes in the concentrations of various carbonyl products: benzoic anhydride (at 1780 cm^{-1}), phenyl benzoate (1740 cm^{-1}) and fluorenone (1718 cm^{-1}), and various hydroxyl products: phenols (3650 cm^{-1}) and benzoic acid (3525 cm^{-1}), during the thermal ageing of PEEK in air between 250 and 320 °C. As expected, temperature accelerates the oxidation kinetics of PEEK.

Two ageing indicators were determined graphically for all the kinetic curves. They are: the induction time (t_i) marking the onset of the auto-acceleration stage, and the maximum oxidation rate (r_{ox}) corresponding to the maximum slope of the kinetic curves. These two indicators obey an Arrhenius law between 250 and 320 °C. Despite the results dispersion, the activation energies of t_i and r_{ox} are of the same order of magnitude for all the degradation products. As an example, Table 1 summarizes the values of the activation energy found in air. The average values, which characterize the oxidation kinetics of PEEK under these exposure conditions, are: 113 ± 21 kJ mol^{-1} for t_i, and 160 ± 17 kJ mol^{-1} for r_{ox}.

The maximum rates of accumulation of phenyl benzoate and fluorenone in air in molten state, typically between 400 and 485 °C, have been already determined in the literature [2]. Their values are reported in the Arrhenius diagram of Fig. 6 where they are compared with the rates determined for these two products in air in rubbery state (between 250 and 320 °C in the present study). Two distinct behaviors are clearly put in evidence on both sides of the melting point (T_m ≈ 343 °C) of PEEK. In rubbery state, the two degradation products accumulate with very close rates, whereas in molten state, their accumulation rates differ substantially, this gap increasing with the temperature. In addition to a jump of the pre-exponential factor, mainly due to the transformation of the crystalline phase into the amorphous phase, a slope rupture is clearly observed in the Arrhenius graph of r_{ox}

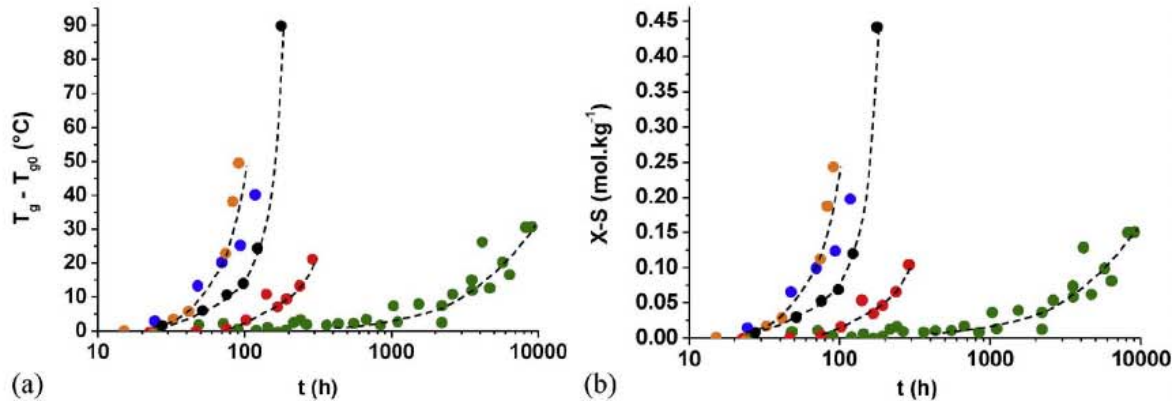

Fig. 18. Differences between the glass transition temperature and its initial value (T_g - T_{g0}) (a) and between the numbers of crosslinking and chain scission events (X - S) (b) during the thermal ageing of PEEK under an oxygen pressure of 0.21 bar (in green), 3 bars (red), 8 bars (black), 10 bars (blue) and 20 bars (orange) at 250 °C. (For interpretation of the references to colour in this figure legend, the reader is referred to the Web version of this article.)

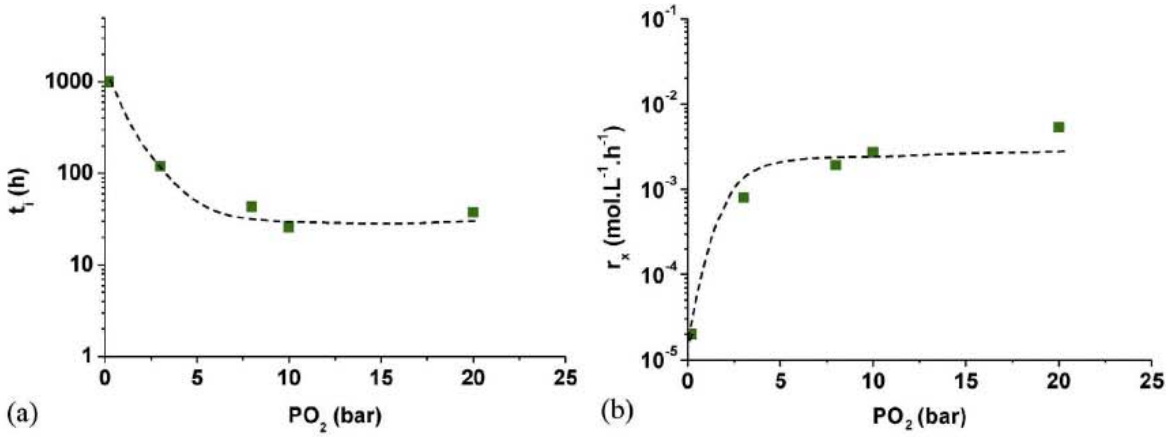

Fig. 19. Changes in the induction time (a) and the maximum rate (b) of crosslinking with oxygen partial pressure at 250 °C.

Table 5
Critical pressure (P_C), induction time (t_i) and maximum rate (r) for molar and macromolecular modifications in oxygen excess at 250 °C.

	P_C (bars)	t_i in O_2 excess (h)	r in O_2 excess (mol.L^{-1}.h^{-1})
Crosslinking	5	36	33.3×10^{-4}
Benzoic anhydride	5	65	19.7×10^{-4}
Phenyl benzoate	5	30	13.1×10^{-4}
Fluorenone	5	30	13.1×10^{-4}

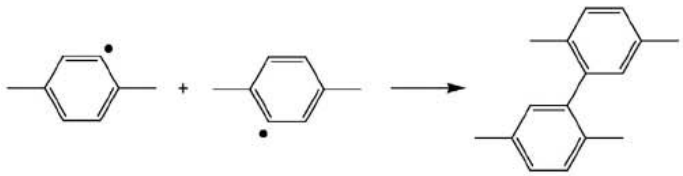

Fig. 20. Crosslinking mechanism of PEEK by intermolecular coupling of phenyl radicals [3–6].

when passing T_m for phenyl benzoate. In contrast, for fluorenone, the slope remains almost the same. The activation energies found for these two degradation products on both sides of T_m are reported in Table 2.

A more careful analysis of the carbonyl region shows an inversion in the relative predominance of the IR absorption bands of phenyl benzoate (at 1740 cm^{-1}) and fluorenone (1718 cm^{-1}) when passing T_m (Fig. 7). In their study, Cole and Casella [2] had already shown a predominance of phenyl benzoate over fluorenone at 400 °C and the reverse behavior at higher temperatures (typically between 430 and 485 °C). To explain this behavioral inversion, they had assumed a diffusion control of oxidation in PEEK films of 50 µm thickness above 430 °C. In contrast, at 400 °C, the oxidation would be slow enough to allow oxygen to diffuse up to the film core. In this case, phenyl benzoate, which is only formed in the presence of oxygen, would be present throughout the film thickness and thus, would become the major degradation product. However, this assumption does not explain the complete disappearance of phenyl benzoate above T_m.

However, it is well known that some chemical reactions, in particular the recombinations of radical species, are favored by an increase in the molecular mobility when passing a physical transition. Unfortunately, the literature does not provide a mechanism for the formation of phenyl benzoate. One possibility, however, would be the termination by coupling of carboxyl and phenoxyl radicals (Fig. 8) whose the origins will be detailed later in this document. This reaction requires the rearrangement of the phenyl radical in the form of a quinone. Of course, it is in competition with the diffusion of these two radicals out of the cage, which will lead to the formation of a wide variety of degradation products (benzoic acid, carbon dioxide, phenols, etc.). It is expected that an increase in temperature promotes diffusion and thus, reduces significantly the formation yield of phenyl benzotate, as previously seen in Fig. 6.

To evidence the influence of the oxygen partial pressure on the oxidation kinetics of PEEK, FTIR analyzes were performed on PEEK films aged under oxygen partial pressures ranged between 0.21 (in air)

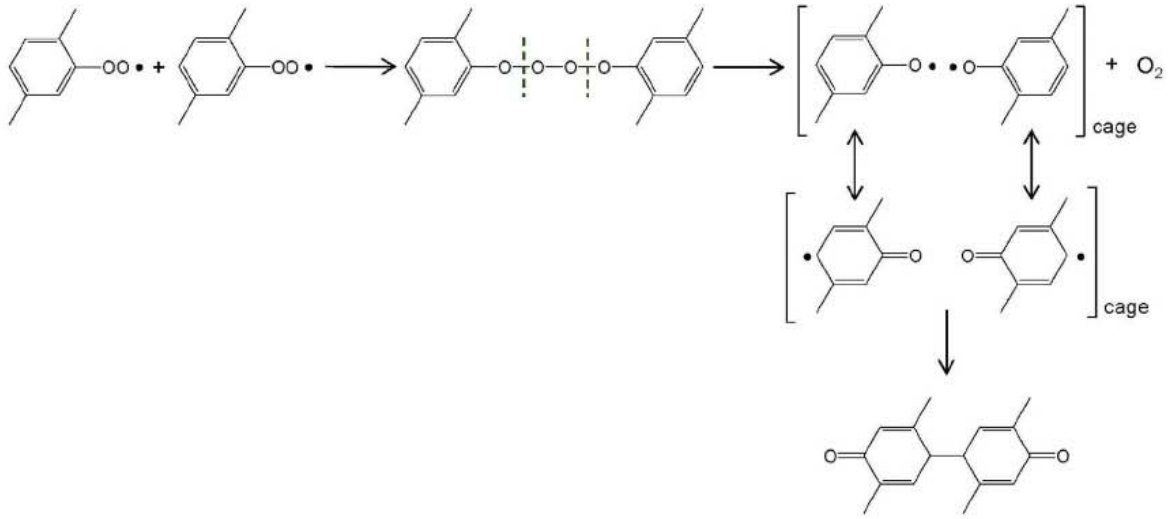

Fig. 21. Crosslinking mechanism of PEEK by intermolecular coupling of peroxy radicals.

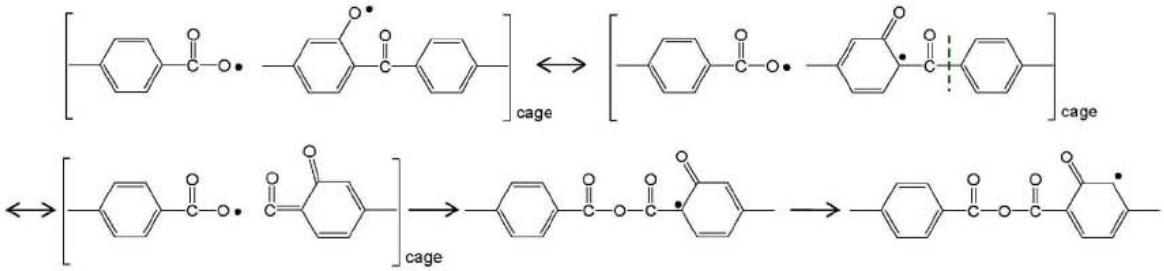

Fig. 22. Formation of benzoic anhydride by coupling of carboxyl and phenoxyl radicals.

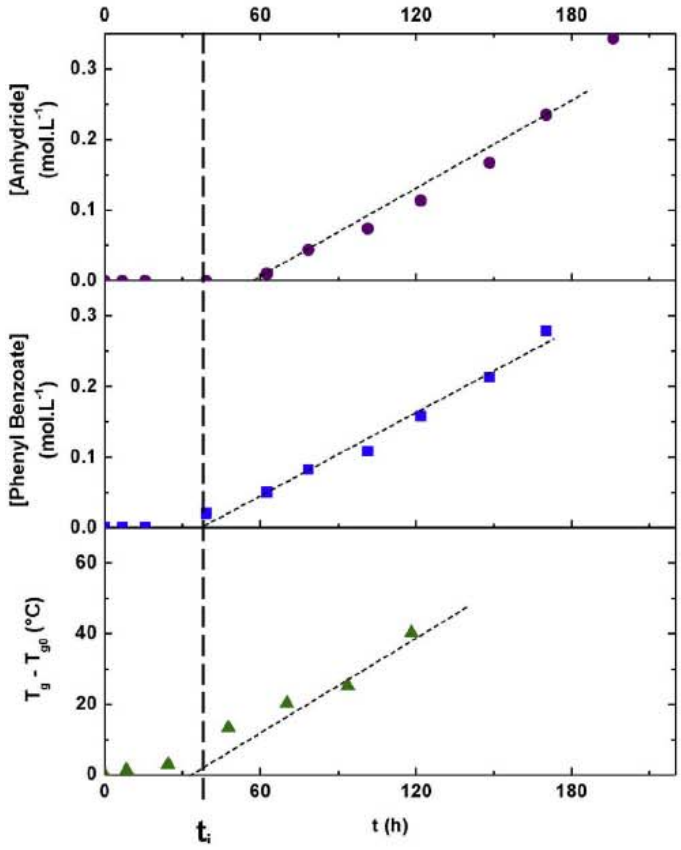

Fig. 23. Comparison of the changes in the concentrations of benzoic anhydride (●) and phenyl benzoate (■) with the changes in the glass transition temperature (▲) during the thermal ageing of PEEK under 10 bars of oxygen at 250 °C.

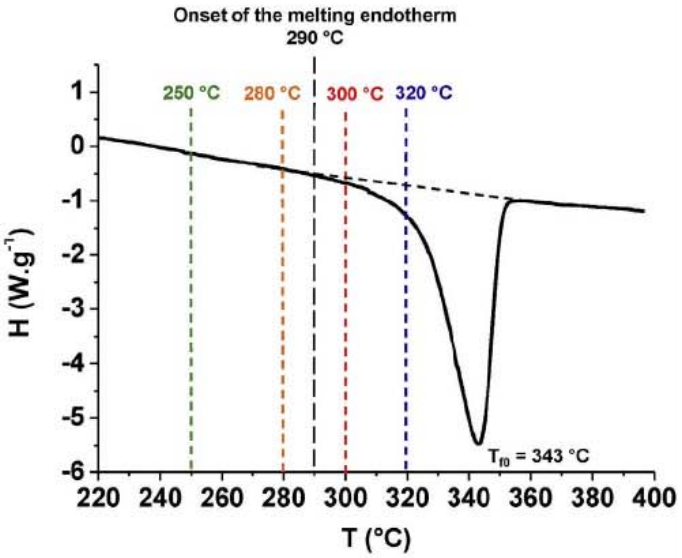

Fig. 25. DSC thermogram of PEEK before ageing. Positioning of the thermal ageing temperatures on both sides of the onset of the melting endotherm.

and 50 bars, between 180 and 250 °C. As an example, Fig. 9 and Fig. 10 report the changes in the concentrations of the various carbonyl (benzoic anhydride, phenyl benzoate and fluorenone) and hydroxyl products (phenols and benzoic acid) during the thermal ageing of PEEK under different oxygen partial pressures at 250 °C. It is clear that the oxygen partial pressure accelerates the oxidation kinetics of PEEK. Benzoic anhydride and phenyl benzoate are the two major degradation products under high oxygen partial pressure. In contrast, phenols and benzoic acid are formed in very low concentrations, whatever the oxygen partial pressure.

As an example, the values of t_i and r_{ox} determined for benzoic

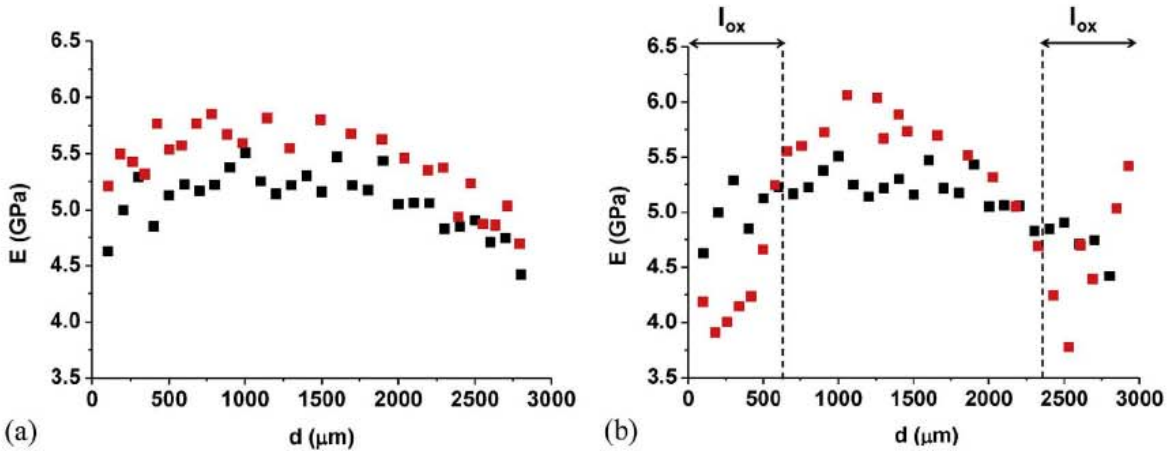

Fig. 24. Profiles of the Young's modulus in the thickness of the PEEK plate before (in black) and after (red) 3166 h of exposure in air at 280 °C (a) and 645 h of exposure in air at 300 °C (b). (For interpretation of the references to colour in this figure legend, the reader is referred to the Web version of this article.)

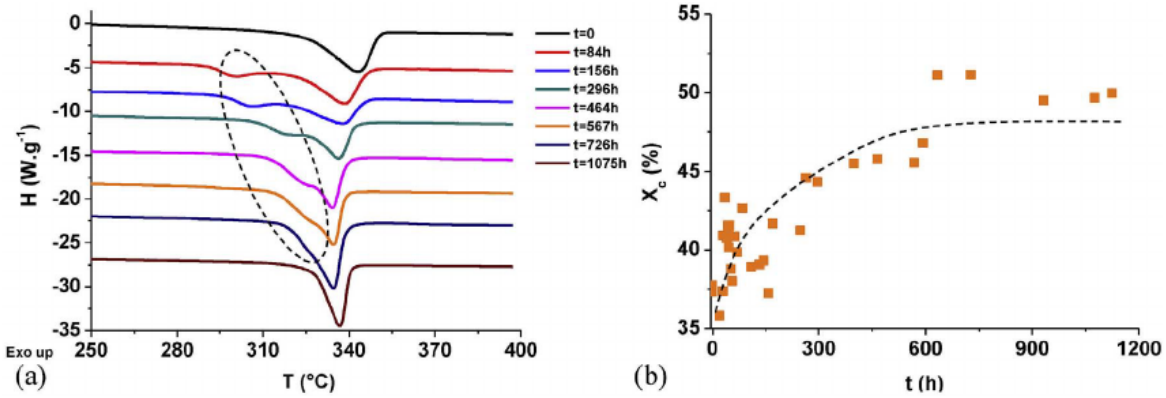

Fig. 26. Modification of the DSC thermogram (a) and changes in the crystallinity ratio (b) during the thermal ageing of PEEK films in air at 280 °C.

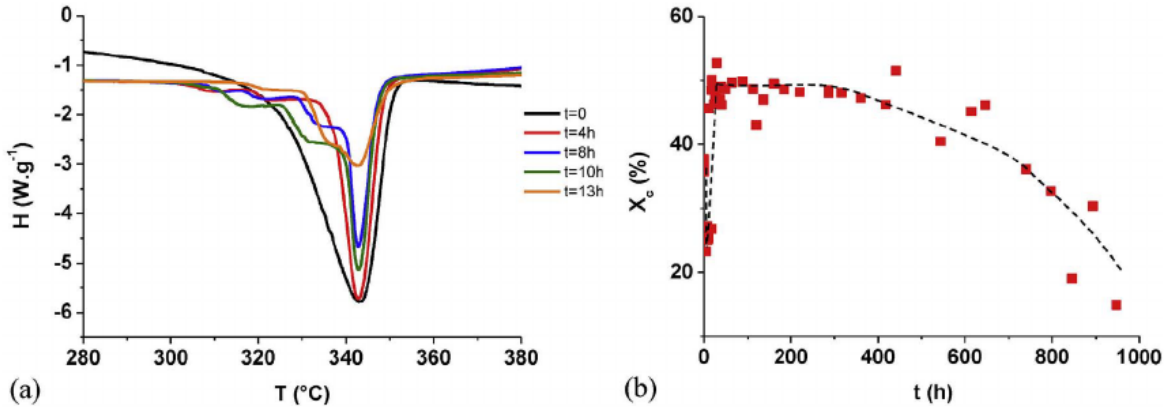

Fig. 27. Modification of the DSC thermogram (a) and changes in the crystallinity ratio (b) during the thermal ageing of PEEK films in air at 300 °C.

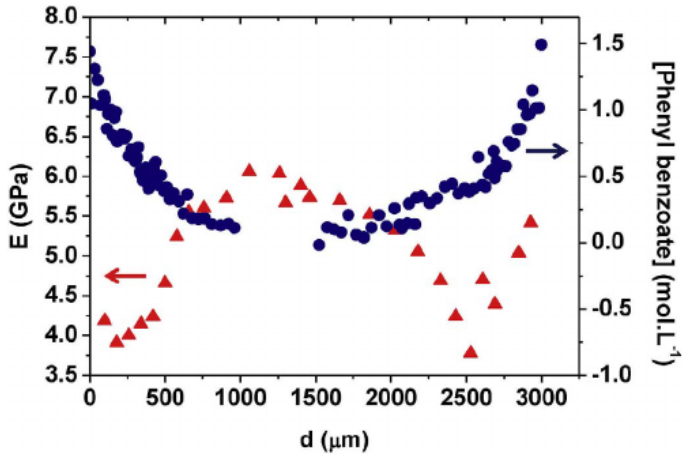

Fig. 28. Comparison of the degradation profiles determined in the thickness of a PEEK plate by FTIR spectrophotometry (●) and micro-indentation (▲) after 645 h of exposure in air at 300 °C.

anhydride, phenyl benzoate and fluorenone at 250 °C were plotted as a function of the oxygen partial pressure in Fig. 11. If the values of t_i are comparable, in contrast, the values of r_{ox} rank in the importance order reported previously for the carbonyl products (Fig. 9), i.e.: phenyl benzoate > benzoic anhydride ≫ fluorenone.

It is found that the curves exhibit a hyperbolic shape and reach a plateau, which is a characteristic of the oxygen excess regime, under high oxygen partial pressures. In other words, t_i and r_{ox} become almost independent of the oxygen partial pressure above a critical value, denoted P_C.

The values of P_C, as well as the values of t_i and r_{ox} in oxygen excess, determined at 220 and 250 °C are summarized in Table 3. It is noteworthy that the oxygen excess is not yet reached under 50 bars of oxygen at 180 and 200 °C. Nevertheless, it appears clearly that P_C is a decreasing function of temperature. Thus, between 180 and 250 °C, all the ageing experiments made in air correspond to a regime in oxygen default.

All these experimental results allow proposing a mechanism of thermal degradation for PEEK. As already proposed in the literature [2–4], this mechanism is initiated by the breakdown of ketone and ether bonds of the monomer unit and thus, leads to the formation of three main types of radical species (Fig. 12): acyl ($P_1^{\bullet}$), phenoxyl ($P_2^{\bullet}$) and phenyl radicals ($P_3^{\bullet}$ or $P_4^{\bullet}$). First of all, the acyl radicals are responsible for the formation of carbon monoxide (CO) by decarbonylation, but also benzaldehyde by hydrogen abstraction on aromatic rings. Because of the low dissociation energy of the CH bond in an aldehyde group ($E_D = 375\ kJ\ mol^{-1}$ [20], against $E_D = 393\ kJ\ mol^{-1}$ in a methylene group), it is expected that benzaldehyde oxidizes almost instantaneously into benzoic acid. Therefore, it is not surprising that this carbonyl product is not detected by FTIR spectrophotometry [21]. In contrast, the phenoxyl radicals lead to the formation of phenols by hydrogen abstraction on aromatic rings. Like phenolic stabilizers [22], they can also be stabilized by resonance to form quinone species.

Thus, the propagation of oxidation is composed of two stages. First of all, the formation of peroxy radicals by oxygen addition onto acyl and phenyl radicals. Then, the formation of hydroperoxides (POOH) by hydrogen abstraction on aromatic rings by peroxy radicals (Fig. 13). Let us recall that, at high temperature (typically for T > 200 °C), the decomposition of hydroperoxides is exclusively unimolecular [23].

The hydroperoxides resulting from the oxidation of acyl radicals are responsible for the formation of benzoic acid. Indeed, their decomposition generates carbonyl radicals which can either recombine by hydrogen abstraction on aromatic rings and thus, give the benzoic acid, or rearrange to form carbon dioxide (CO_2) by decarboxylation

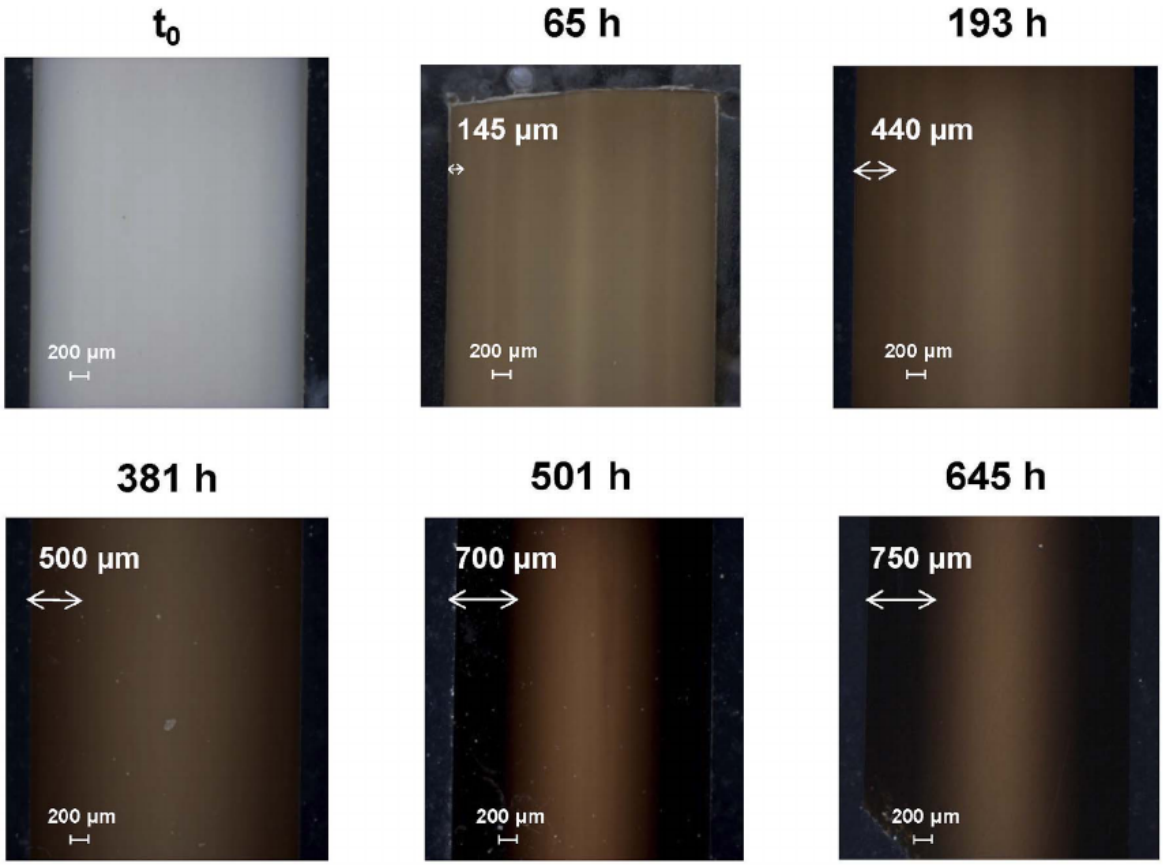

Fig. 29. Examination by optical microscopy (with a magnification of × 2,5) of the superficial oxidized layer of PEEK after different durations of exposure in air at 300 °C.

Table 6
Average thickness of oxidized layer of PEEK determined by micro-indentation, FTIR spectrophotometry or optical microscopy after different durations of exposure in air at 280 and 300 °C.

T (°C)	t (h)	l_{ox} (µm)
280	381	105 ± 15
	1317	415 ± 15
	2492	620 ± 30
	3166	650 ± 25
300	65	145 ± 15
	193	440 ± 25
	381	475 ± 50
	501	685 ± 25
	645	700 ± 50

(Fig. 14a). Concerning phenols, they come from phenoxyl radicals generated by the thermolysis (Fig. 12), but also by the decomposition of the hydroperoxides resulting from the oxidation of phenyl radicals (Fig. 14b).

As already proposed in the literature [2,6], the termination reaction by intramolecular coupling of phenyl radicals allows explaining the formation of fluorenone in oxygen default (Fig. 15). However, this degradation product is also present, although in a smaller quantity, under high oxygen partial pressure. A second termination reaction, by intramolecular coupling of peroxy radicals, was thus proposed in this study for accounting for such a behavior (Fig. 16).

3.2. Changes in macromolecular structure

The molecular mass is the structural variable commonly used for monitoring the changes in the macromolecular architecture of the polymer, i.e. chain scissions (denoted S) and crosslinking events (denoted X), during its chemical ageing. As each chain scission leads to a chain formation, whereas each crosslinking event leads to a chain disppearance, it can be written:

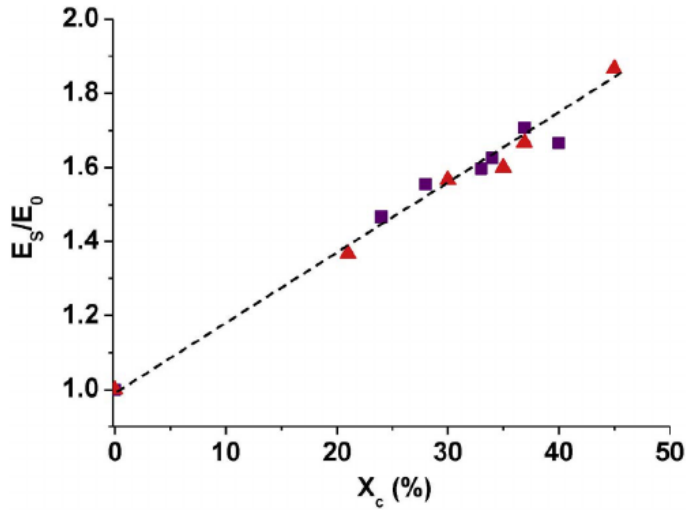

Fig. 30. Changes in the Young's modulus of PEEK (normalized by the Young's modulus of its amosphous phase) with crystallinity ratio. Comparison of the values determined by micro-indentation in the present study (▲) and uniaxial tensile testings in the literature [33,34] (■).

$$S - X = \frac{1}{M_n} - \frac{1}{M_{n0}} \tag{7}$$

where M_{n0} and M_n are the number average molecular masses before and after ageing respectively.

However, it was impossible to monitor the changes in the molecular mass of PEEK during its thermal ageing by a direct classical chromatographic (CES or GPC) or viscometric (in solution) method, because

this polymer is not soluble in usual solvents (acetone, toluene, ethyl acetate, etc.). It was thus necessary to use an indirect method having already proved its worth for this polymer [10]: differential scanning calorimetry (DSC). Indeed, DSC gives access to the value of M_n if knowing the value of T_g and applying the Fox-Flory's relationship [24]:

$$T_g - T_{g0} = -k_{FF}\left(\frac{1}{M_n} - \frac{1}{M_{n0}}\right) \quad (8)$$

where k_{FF} is the Fox-Flory's constant (expressed in $K.mol.kg^{-1}$), which is an increasing function of the chain stiffness.

The value of k_{FF} was determined from the glass transition temperatures and molecular masses of several grades of PEEK kindly supplied by Victrex. Indeed, the slope of the curve $T_g = f(1/M_n)$ gives access to the value of k_{FF}, while the ordinate at the origin corresponds to the value of $T_{g\infty}$ (i.e. to the theoretical value of T_g for a linear polymer having the same chemical structure but an infinite molecular mass). Thus, for PEEK Victrex, it was found: $k_{FF} = 204\ K\,kg\,mol^{-1}$ and $T_{g\infty} = 432\ K$. It is noteworthy that this last value is very close to the theoretical value ($T_{g\infty} = 433\ K$) calculated according to the molar additivity law proposed by Van Krevelen in his book [25].

By combining Eq. (7) and Eq. (8), the following relationship was obtained between T_g and the numbers of chain scissions and crosslinking events:

$$T_g - T_{g0} = k_{FF}(X - S) \quad (9)$$

It can be seen that T_g decreases with the number of chain scissions, but increases with the number of crosslinking events.

Fig. 17 reports the differences between T_g and its initial value (T_g - T_{g0}) and between the numbers of crosslinking and chain scission events (X - S) for PEEK films exposed in air between 250 and 320 °C. It appears clearly that crosslinking predominates largely over chain scissions in rubbery state. Let us recall that this relative predominance had been already observed by several authors in molten state [3–5,7–9]. In addition, crosslinking is highly thermo-activated.

The values of the induction time (t_i) and the maximum rate of crosslinking (r_x) were determined graphically for all of these kinetic curves. In a first approach, chain scissions were neglected with respect to crosslinking, which allowed rewriting Eq. (9) such as:

$$r_x = \frac{dX}{dt} = \frac{1}{k_{FF}} \times \frac{dT_g}{dt} \quad (10)$$

These two indicators obey an Arrhenius law between 250 and 320 °C. The values of activation energy are reported in Table 4 where they are compared to the values obtained for carbonyl products. They are all of the same order of magnitude.

DSC analyzes were also carried out on PEEK films after thermal ageing at 250 °C under different oxygen partial pressures ranged between 0.21 and 20 bars. The changes in (T_g - T_{g0}) and (X - S) are given in Fig. 18. It is found the same behavior as in air. In a general way, oxygen partial pressure accelerates the crosslinking kinetics up to a critical pressure of about 5 bars at 250 °C, a value which has been already determined by FTIR spectrophotometry.

The values of t_i and r_x determined at 250 °C were plotted as a function of the oxygen partial pressure in Fig. 19. It can be seen that the curves exhibit a hyperbolic shape and reach a plateau, which is a characteristic of the oxygen excess regime, above $P_C = 5$ bars. The values of t_i, r_S and r_X in oxygen excess at 250 °C are summarized in Table 5 where they are compared to the values obtained for the carbonyl products. They are all of the same order of magnitude. It is deduced that the crosslinking is a direct consequence of the PEEK oxidation.

As already proposed in the literature [3–6], the termination by intermolecular coupling of phenyl radicals is the main crosslinking mechanism in oxygen default (Fig. 20). However, this reaction cannot explain the crosslinking of PEEK in oxygen excess since, in these exposure conditions, all the $P^{\bullet}$ radicals have been almost instantaneously transformed into $PO_2^{\bullet}$ radicals.

One possibility would be the termination by intermolecular coupling of peroxy radicals. Indeed, this reaction involves, first of all, the formation of a very unstable tetraoxide bridge (POOOOP) which decomposes almost instantaneously at high temperature (in particular, above 150 °C) to give two $PO^{\bullet}$ radicals and oxygen. However, the $PO^{\bullet}$ radicals can rearrange to finally couple and thus, form a crosslinking node, as illustrated in Fig. 21.

There are other crosslinking mechanisms which may occur throughout the whole range of oxygen partial pressure. The formation mechanism of phenyl benzoate has been already mentioned in section 3.1 (Fig. 8). However, this mechanism does not lead to a tetrafunctional (in “X”), but to a trifunctional crosslinking node (in “T”). Another mode of rearrangement of the phenoxyl radical can be envisaged: it involves the breakdown of a ketone bond before coupling with the carboxyl radical to finally give benzoic anhydride (Fig. 22). However, in this case, it is not obtained a crosslinking node, but the macromolecular chain is reformed.

No doubt, these two mechanisms play a major role at the macromolecular scale, as shown in Fig. 23. Indeed, there is clearly a correlation between the accumulations of phenyl benzoate and benzoic anhydride and the increase in T_g. In addition, the accumulation rates of these two products are of the same order of magnitude as the crosslinking rate.

3.3. Consequences of oxidation on elastic properties

The profiles of elastic modulus generated by oxidation in the thickness of PEEK plates of 3 mm thickness were determined by micro-indentation. As an example, the profiles obtained before and after 3166 h of exposure in air at 280 °C, and before and after 645 h of exposure in air at 300 °C, are reported in Fig. 24. It can be seen that the initial profile is not exactly flat. Indeed, the elastic modulus is slightly smaller in the superficial layers of the samples due to a lower crystallinity (of 30%, against 41% in the core), resulting from the inhomogeneous cooling of the samples (temperature gradient in the sample thickness) after their processing by injection moulding. Nevertheless, an average value of the elastic modulus E_S was calculated for the non-aged PEEK: it is equal to 5.0 ± 0.5 GPa. This value is slightly higher than the Young's modulus determined by uniaxial tensile testing on dumbbell specimens: 4.2 ± 0.1 GPa. For this reason, in the present study, a corrective factor of 0.84 has been systematically applied to the indentation modulus in order to access the value of the Young's modulus.

During thermal ageing, the micro-indentation reveals two distinct types of behavior on each side of the onset of the melting endotherm, i.e. on each side of $T_{m\ onset} \approx 290$ °C (see Fig. 25).

When $T < 290$ °C, the Young's modulus increases slowly throughout the sample thickness (Fig. 24a). This increase is mainly attributed to the annealing phenomenon [26–30], although the chemicrystallization phenomenon cannot be completely excluded. Indeed, the increase in molecular mobility favors the crystallization of the macromolecular chains in the amorphous phase located at the vicinity of nuclei or small crystals, which are almost undetectable by DSC. Anyway, annealing manifests by the appearance of a secondary melting endotherm centered about 20 °C above the exposure temperature on the DSC thermograms. This peak shifts gradually towards higher temperatures to finally integrates into the main melting endotherm (Fig. 26a). As a result, the global crystallinity ratio increases up to a maximum value of about 50% (Fig. 26b). X-ray diffraction analyzes in real-time (i.e. at the exposure temperature) would certainly help us to better understand the origin and growth of these new crystals.

When $T > 290$ °C, it can be seen an increase in the Young's modulus in the sample core, but also a decrease in the Young's modulus in the superficial oxidized layer (Fig. 24b). Here again, the increase of Young's modulus in the sample core is mainly attributed to the

annealing phenomenon. Indeed, at these temperatures, the smallest crystals (i.e. the less perfect crystals) melt and thus, increase the fraction of amorphous phase able of better crystallizing. It can be seen that the “low temperature” part of the melting endotherm disappears almost instantaneously and, in return, its “high-temperature” part grows gradually. As a result, the crystallinity ratio increases up to a maximum value of the order of 50%. It is noteworthy that, in the absence of oxygen, the chain scissions occurring at the ketone and ether bonds (Fig. 12) destroy gradually the entanglement network in the amorphous phase and thus, liberate short macromolecular segments which will easily migrate up to the surface of the remaining crystals and integrate them [31,32]. From this point of view, chain scissions favor the annealing of the PEEK matrix.

In contrast, in the presence of oxygen, let us recall that crosslinking predominates largely over chain scissions. At the end of an induction period of approximately 100 h in air at 300 °C (see Fig. 17), crosslinking reduces considerably the molecular mobility in the PEEK matrix and thus, finds in opposition with the annealing phenomenon. As a result, the crystallinity ratio returns progressively to its initial value (Fig. 27b).

It should be noted that the decrease in the Young's modulus in the oxidized layer correlates perfectly with changes in the macromolecular architecture of PEEK, in particular with the accumulation of phenyl benzoate determined by FTIR spectrophotometry in an ATR mode (Fig. 28).

In addition, it should be noted that the thicknesses of oxidized layer determined by these two techniques (micro-indentation and FTIR spectrophotometry) are comparable. They are of the same order of magnitude as the thicknesses of the brownish layer observed by optical microscopy on the free edges of the samples. As an example, Fig. 29 shows the micrographs obtained after four different times of exposure in air at 300 °C. It is clear that oxidation results in a browning of PEEK.

The average values of the thickness of oxidized layer determined in air at 280 and 300 °C with these three techniques are summarized in Table 6.

Finally, a correlation was established between the Young's modulus and the crystallinity ratio. The average values E_S of the Young's modulus of the PEEK plates aged in air at 280 and 300 °C were calculated with Eq. (6) from the micro-indentation profiles. These values were plotted as a function of the crystallinity ratio X_C in Fig. 30, where they are compared with the few data of uniaxial tensile testings available in the literature [33,34]. It can be seen that all the points are placed around a single master straight-line of equation:

$$\frac{E_S}{E_0} = 1 + 1,\ 83.10^{-2} \times X_c \tag{11}$$

where E_0 is the Young's modulus of the amorphous phase of PEEK. E_0 = 3 GPa in micro-indentation [17] and E_0 = 2,5 GPa in uniaxial tensile [34].

In fact, this equation satisfies the Tobolsky's relationship [35]:

$$E_S = E_0 + b \times \frac{\Delta H_{f0} \times M}{V} \times X_c \tag{12}$$

where M is the molar mass and V is the molar volume of the monomer unit, ΔH_{f0} is the melting enthalpy of crystal and b is an unitless constant.

Let us recall that: $M = 288\ g\ mol^{-1}$, $V = 206\ cm^3\ mol^{-1}$ and $\Delta H_{f0} = 130\ J\ g^{-1}$ for PEEK [16]. By equalizing Eq. (11) and Eq. (12), it comes finally: b = 25.

4. Conclusion

The thermal degradation of the PEEK matrix has been studied in rubbery state between 180 and 320 °C under oxygen partial pressures ranged between 0.21 and 50 bars, i.e. domains of temperature and oxygen partial pressure almost completely unexplored. The analysis at the molecular scale, by FTIR spectrophotometry, has allowed identifying the main degradation products which accumulate in the PEEK matrix and elucidate partly the thermolysis and thermo-oxidation mechanisms. These products are benzoic anhydride (at 1780 cm^{-1}), phenyl benzoate (1740 cm^{-1}), fluorenone (1718 cm^{-1}), phenols (3650 cm^{-1}) and benzoic acid (3525 cm^{-1}). Benzoic anhydride and phenyl benzoate are the two major products under high oxygen partial pressure. They come from the termination by coupling of the carboxyl and phenoxyl radicals.

The analysis at the upper scales, by DSC and then micro-indentation, has allowed showing, on the one hand, that crosslinking predominates largely over chain scissions whatever the exposure conditions. In solid state, annealing takes place throughout the sample thickness, leading to an increase in both the crystallinity ratio and the Young's modulus. On the other hand, above the onset of the melting endotherm (i.e. when T > 290 °C), crosslinking reduces considerably the molecular mobility in the oxidized layer, thus preventing the annealing phenomenon and causing the decrease in both the crystallinity ratio and Young's modulus. In all cases, the Young's modulus and the crystallinity ratio correlate perfectly. In fact, their values check the Tobolsky's relationship.

In a next communication, a kinetic model will be derived from the oxidation mechanistic scheme established for PEEK, and it will be interfaced with the different structure/property relationships (in particular, with Eq. (9) and Eq. (12)) identified in this study. This theoretical tool will allow us predicting not only the degradation state of PEEK, but also the changes in its thermomechanical properties during thermal ageing. The validity of this tool will be checked from all the experimental data collected in this study.

References

[1] X. Colin, G. Teyssèdre, M. Fois, Ageing and degradation of multiphase polymer systems, in: A. Boudenne, L. Ibos, Y. Candau, S. Thomas (Eds.), Handbook of Multiphase Polymer Systems, 2/2 John Wiley & Sons Ltd, Chichester, 2011, pp. 797–841 Chap. 21.

[2] K.C. Cole, I.G. Casella, Fourier transform infrared spectroscopic study of thermal degradation in films of poly(etheretherketone), Thermochim. Acta 211 (1992) 209–228.

[3] M. Day, D. Sally, D.M. Wiles, Thermal degradation of poly(aryl-ether-ether-ketone): experimental evaluation of crosslinking reactions, J. Appl. Polym. Sci. 40 (9–10) (1990) 1615–1625.

[4] J.N. Hay, D.J. Kemmish, Thermal decomposition of poly(aryl ether ketones), Polymer 28 (12) (1987) 2047–2051.

[5] A. Jonas, R. Legras, Thermal stability and crystallization of poly(aryl ether ether ketone), Polymer 32 (15) (1991) 2691–2706.

[6] P. Patel, T.R. Hull, R.W. McCabe, D. Flath, J. Grasmeder, M. Percy, Mechanism of thermal decomposition of poly(ether ether ketone) (PEEK) from a review of decomposition studies, Polym. Degrad. Stabil. 95 (5) (2010) 709–718.

[7] C. Nicodeau, Modélisation du soudage en continu de composites à matrice thermoplastique. PhD thesis, ENSAM, Paris, 2005.

[8] M. Day, T. Suprunchuk, J.D. Cooney, D.M. Wiles, Thermal degradation of poly(aryl-ether–ether-ketone) (PEEK): a differential scanning calorimetry study, J. Appl. Polym. Sci. 36 (5) (1988) 1097–1106.

[9] K.L. White, L. Jin, N. Ferrer, M. Wong, T. Bremner, H.J. Sue, Rheological and thermal behaviors of commercial poly(aryletherketone)s, Polym. Eng. Sci. 53 (3) (2013) 651–661.

[10] E. Richaud, P. Ferreira, L. Audouin, X. Colin, J. Verdu, C. Monchy-Leroy, Radiochemical ageing of poly(ether ether ketone), Eur. Polym. J. 46 (4) (2010) 731–743.

[11] S. Giancaterina, A. Rossi, A. Rivaton, J.L. Gardette, Photochemical evolution of poly (ether ether ketone), Polym. Degrad. Stabil. 68 (1) (2000) 133–144.

[12] S. Commereuc, D. Vaillant, J.L. Philippart, J. Lacoste, J. Lemaire, D.J. Carlsson, Photo and thermal decomposition of iPP hydroperoxides, Polym. Degrad. Stabil. 57 (1997) 175–182.

[13] D.J. Carlsson, R. Brousseau, D.M. Wiles, Reactions of sulfur dioxide with oxidized polyolefins, Polym. Degrad. Stabil. 15 (1986) 67–79.

[14] D.J. Carlsson, D.M. Wiles, The photodegradation of polypropylene films. II. Photolysis of ketonic oxidation products, Macromolecules 2 (6) (1969) 587–597.

[15] F. Gugumus, Formation of ester functional groups in oxidizing polymers, Polym. Degrad. Stabil. 65 (1) (1999) 5–13.

[16] D.J. Blundell, B.N. Osborn, The morphology of poly(aryl-ether-ether-ketone), Polymer 24 (8) (1983) 953–958.

[17] T. Iqbal, B.J. Briscoe, P.F. Luckham, Surface plasticization of poly(ether ether ketone), Eur. Polym. J. 47 (12) (2011) 2244–2258.

[18] W.C. Oliver, G.M. Pharr, An improved technique for determining hardness and elastic modulus using load and displacement sensing indentation experiments, J.

Mater. Res. 7 (6) (1992) 1564–1583.
[19] S. Collin, P.O. Bussière, S. Thérias, J.M. Lambert, J. Perdereau, J.L. Gardette, Physicochemical and mechanical impacts of photo-ageing on bisphenol a polycarbonate, Polym. Degrad. Stabil. 97 (11) (2012) 2284–2293.
[20] S.J. Blanksby, G.B. Ellison, Bond dissociation energies of organic molecules, Acc. Chem. Res. 36 (4) (2003) 255–263.
[21] L.K. Nait-Ali, X. Colin, A. Bergeret, Kinetic analysis and modelling of PET macromolecular changes during its mechanical recycling by extrusion, Polym. Degrad. Stabil. 96 (2) (2011) 236–246.
[22] J. Pospíšil, Chemical and photochemical behaviour of phenolic antioxidants in polymer stabilization: a state of the art report, part II, Polym. Degrad. Stabil. 39 (1) (1993) 103–115.
[23] X. Colin, L. Audouin, J. Verdu, Determination of thermal oxidation rate constants by an inverse method. Application to polyethylene, Polym. Degrad. Stabil. 86 (2) (2004) 309–321.
[24] T.G. Fox, P.J. Flory, Second-order transition temperatures and related properties of polystyrene. I. Influence of molecular weight, J. Appl. Phys. 21 (6) (1950) 581–591.
[25] D.W. Van Krevelen, K. Te Nijenhuis, Properties of Polymers, fourth ed., Elsevier, Amsterdam, 2009.
[26] D.J. Blundell, On the interpretation of multiple melting peaks in poly(ether ether ketone), Polymer 28 (13) (1987) 2248–2251.
[27] G.M.K. Ostberg, J.C. Seferis, Annealing effects on the crystallinity of polyetheretherketone (PEEK) and its carbon fiber composite, J. Appl. Polym. Sci. 33 (1) (1987) 29–39.
[28] D.C. Bassett, R.H. Olley, I.A.M. Al Raheil, On crystallization phenomena in PEEK, Polymer 29 (10) (1988) 1745–1754.
[29] P. Cebe, Annealing study of poly(etheretherketone), J. Mater. Sci. 23 (10) (1988) 3721–3731.
[30] M. Buggy, A. Carew, The effect of thermal ageing on carbon fibre-reinforced polyetheretherketone (PEEK) - Part II Morphological changes, J. Mater. Sci. 29 (8) (1994) 2255–2259.
[31] M.S. Rabello, J.R. White, Crystallization and melting behaviour of photodegraded polypropylene - I. Chemi-crystallization, Polymer 38 (26) (1997) 6379–6387.
[32] B. Fayolle, E. Richaud, X. Colin, J. Verdu, Review: degradation-induced embrittlement in semi-crystalline polymers having their amorphous phase in rubbery state, J. Mater. Sci. 43 (22) (2008) 6999–7012.
[33] T. Nishino, K. Tada, K. Nakamae, Elastic modulus of crystalline regions of poly (ether ether ketone), poly(ether ketone) and poly(p-phenylene sulphide), Polymer 33 (4) (1992) 736–743.
[34] N.D. Albérola, P. Mélé, C. Bas, Tensile mechanical properties of PEEK films over a wide range of strain rates. II, J Appl Polym Sci 64 (6) (1997) 1053–1059.
[35] A.V. Tobolsky, Properties and Structure of Polymers, Wiley, New York, 1960.